Diabetologia
https://doi.org/10.1007/s00125-024-06210-8

ARTICLE

Spatial proteomics of human diabetic kidney disease, from health to class III

Ayano Kondo[1] · Monee McGrady[1] · Dhiraj Nallapothula[2] · Hira Ali[1] · Alexandro E. Trevino[1] · Amy Lam[1] · Ryan Preska[1] · H. Blaize D'Angio[1] · Zhenqin Wu[1] · Lauren N. Lopez[2] · Harshanna K. Badhesha[2] · Chenoa R. Vargas[2] · Achyuta Ramesh[3] · Nasim Wiegley[2] · Seung Seok Han[4] · Marc Dall'Era[5] · Kuang-Yu Jen[6] · Aaron T. Mayer[1] · Maryam Afkarian[2]

Received: 29 January 2024 / Accepted: 30 April 2024

Abstract

Aims/hypothesis Diabetic kidney disease (DKD) is the leading cause of chronic and end-stage kidney disease in the USA and worldwide. Animal models have taught us much about DKD mechanisms, but translation of this knowledge into treatments for human disease has been slowed by the lag in our molecular understanding of human DKD.

Methods Using our Spatial TissuE Proteomics (STEP) pipeline (comprising curated human kidney tissues, multiplexed immunofluorescence and powerful analysis tools), we imaged and analysed the expression of 21 proteins in 23 tissue sections from individuals with diabetes and healthy kidneys (n=5), compared to those with DKDIIA, IIA-B and IIB (n=2 each) and DKDIII (n=1).

Results These analyses revealed the existence of 11 cellular clusters (kidney compartments/cell types): podocytes, glomerular endothelial cells, proximal tubules, distal nephron, peritubular capillaries, blood vessels (endothelial cells and vascular smooth muscle cells), macrophages, myeloid cells, other $CD45^+$ inflammatory cells, basement membrane and the interstitium. DKD progression was associated with co-localised increases in inflammatory cells and collagen IV deposition, with concomitant loss of native proteins of each nephron segment. Cell-type frequency and neighbourhood analyses highlighted a significant increase in inflammatory cells and their adjacency to tubular and αSMA^+ (α-smooth muscle actin-positive) cells in DKD. Finally, DKD progression showed marked regional variability within single tissue sections, as well as inter-individual variability within each DKD class.

Conclusions/interpretation Using the STEP pipeline, we found alterations in protein expression, cellular phenotypic composition and microenvironment structure with DKD progression, demonstrating the power of this pipeline to reveal the pathophysiology of human DKD.

Keywords Diabetic kidney disease · Spatial biology · Tissue proteomics

Abbreviations

αSMA	Alpha smooth muscle actin
CCR6	CC motif chemokine receptor 6
CODEX	Co-detection by indexing
CXCR3	CXC motif chemokine receptor 3
DKD	Diabetic kidney disease
GEC	Glomerular endothelial cells
HSPG	Heparan sulfate proteoglycan
MUC1	Mucin 1
RORγ	RAR-related orphan receptor C
STEP	Spatial TissuE Proteomics

Dhiraj Nallapothula and Hira Ali contributed equally to this study.

Aaron T. Mayer and Maryam Afkarian contributed equally to this study as joint senior authors.

✉ Maryam Afkarian
mafkarian@ucdavis.edu

[1] Enable Medicine, Menlo Park, CA, USA

[2] Division of Nephrology, University of California, Davis, CA, USA

[3] University of California, San Diego, CA, USA

[4] Department of Internal Medicine, Seoul National University College of Medicine, Seoul, South Korea

[5] Department of Urologic Surgery, University of California-Davis Medical Center, Sacramento, CA, USA

[6] Department of Pathology and Laboratory Medicine, University of California- Davis, Sacramento, CA, USA

Published online: 22 July 2024

Research in context

What is already known about this subject?

- Diabetic kidney disease (DKD) is the leading cause of chronic and end-stage kidney disease
- There is a lag in translating our findings from animal models to human disease due to limited molecular understanding of human DKD

What is the key question?

- What are the molecular spatial changes in human DKD?

What are the new findings?

- Using a Spatial TissuE Proteomics (STEP) pipeline, we quantified 21 proteins, and identified 11 cell types, in 23 tissue sections from individuals with diabetes and healthy kidneys vs those with diabetes and DKDIIA, IIA–B, IIB and III
- DKD progression was associated with co-localised increases in inflammatory cells and deposition of collagen IV, and concomitant loss of native nephron proteins
- DKD progression showed marked regional variability within single tissue sections, as well as inter-individual variability within each DKD class

How might this impact on clinical practice in the foreseeable future?

- This study demonstrates the power of this spatial proteomics pipeline to reveal human DKD pathophysiology with the aim of developing novel diagnostic and therapeutic methods

Introduction

Diabetic kidney disease (DKD) remains a significant cause of morbidity and mortality in people with diabetes worldwide [1]. Current diagnostic tests are limited, especially for detection of early disease. Despite recent advances, effective tools for management of advanced disease are also lacking. Expanding our diagnostic and therapeutic tools for DKD requires a detailed understanding of the molecular mechanisms underlying disease progression in humans. Historically, research on DKD molecular pathobiology largely fell into two categories: (1) dissection of DKD pathophysiology in experimental models; and (2) examination of human biofluids to identify putative disease markers. Generation of data to bridge the gap between understanding of human disease and the detailed experimental molecular mechanisms that are available has been a more recent endeavour. The resulting paucity of such data has slowed translation of insights gleaned from experimental DKD studies into clinical interventions. Bulk and single-cell RNA sequencing of human kidneys has begun to fill this gap, allowing researchers to compare how DKD changes gene expression in animal models vs human patients.

More recently, commercialisation of high-parameter in situ molecular profiling technologies [2], such as mass cytometry, multiplexed immunofluorescence and spatial transcriptomics, has made it possible to draw connections between disease progression, in the context of pathological classes, and molecular and cellular states defined by spatially resolved RNA or protein expression in human kidneys. A comprehensive multi-omics examination of human kidney tissue has generated data for a reference atlas for healthy kidneys [3]. One study reported on expression of 23 proteins in kidney tissues from three individuals with DKD [4]. However, it included minimal clinical information or pathological classification. Furthermore, the comparison of DKD kidneys to those from healthy (non-diabetic) individuals left unresolved the question of whether the observed changes were due to diabetes or kidney disease. We report on expression of a 21-protein panel in 23 regions of interest [5] from 12 individuals with diabetes and histologically normal kidneys vs those with DKD classes IIA to III. The results of this study are the first step in generating a molecular companion to clinicopathological DKD classes, preferentially targeting proteins to address our resources to areas with lower data density.

Methods

The objective of this study was to examine changes in protein expression in relevant cell types in human kidneys, as they progressed from healthy to class III DKD. Patients

donating tissue samples signed an informed consent allowing use of their deidentified samples for research. Collection and storage of tissue and data were conducted under the regulatory processes of the University of California Institutional Review Board. The relevant sections in the electronic supplementary material (ESM) Methods give full details on the study design, tissue repository and tissue preparation.

Tissue characterisation

Tissues were characterised by: (1) evaluation of existing donor clinical data by a nephrologist experienced in DKD care (MA); and (2) histopathological examination by an expert renal pathologist (K-YJ) by microscopic examination of the periodic acid Schiff (PAS)-stained sections (ESM Fig. 1a–d) [6]. The tissue microarray used here included 23 tissue sections from 12 individuals with diabetes. Ten kidney tissue sections were from five diabetic individuals with histologically intact kidneys with no evidence of kidney disease, 12 tissue sections were from two individuals each with DKDIIA, IIA-B or IIB, and one tissue biopsy was obtained from an individual with DKDIII (ESM Fig. 1e,f). Further details are given in ESM Methods.

Tissue staining and data acquisition

Antibody conjugation, tissue staining and data acquisition followed the protocols supplied by Akoya Biosciences (USA). Further details are given in ESM Methods.

CODEX data analysis

Biomarker expression masks for compartment-based analysis Six kidney compartments were outlined for region of interest analysis using the Enable Medicine visualiser (ESM Fig. 2): glomeruli, blood vessels, distal tubules, all tubules, collagen IV^+ areas and the interstitium. Manual outlines of glomeruli and blood vessels were used to create binary masks for these two compartments. Three compartments were isolated by creation of binary masks based on thresholding the expression of relevant proteins (mucin 1 [MUC1] for the distal nephron, CXC motif chemokine receptor 3 [CXCR3] for all tubules, and collagen IV for the basement membrane) and morphological fill operations. The proximal tubule compartment was determined by subtracting the distal nephron compartment from the all-tubules compartment. The interstitial compartment was marked by a mask that was created by subtracting the masks of the other five compartments from a mask of the entire tissue region. The masks were used to label the cells by compartment.

Cell proportion analysis Cell proportions were determined across all cell-type clusters and summarised by sample, disease stage and tissue compartment; values were also summarised across disease stage for individual cell types. These data were visualised using stacked bar plots and boxplots ("ggplot2::geom_bar" with 'pos = "fill"' and "ggplot2::geom_boxplot", respectively).

Compartment protein expression Protein expression in glomeruli was calculated by summing signals over the corresponding regions in the images. For each single channel image, lower and upper intensity thresholds were determined based on the histogram of pixel intensities. Next, the image was min–max-normalised according to these thresholds. The normalisation process was performed to ensure that images from different regions/acquisitions would have the same dynamic range. Further details on co-detection by indexing (CODEX) data analysis are given in ESM Methods.

Results

Patient characteristics

The majority of the 12 donors were self-reported non-Hispanic white individuals with type 2 diabetes (Table 1). All classes, except DKDIIB and III, included kidney tissue from self-reported women and men. Hypertension was present in four of the five donors with diabetes mellitus and healthy kidneys and in all donors with DKD. Nephrectomies were performed between 2010 and 2019, with storage durations as specified in Table 1. eGFR, measured by CKD-EPI [7] from available serum creatinine values, and urine protein (urinalysis) were obtained before nephrectomy if possible or afterwards if not.

Visualising spatial distribution of 21 proteins in human kidneys

Tissue expression of 21 proteins (ESM Table 1) was measured in 23 regions of interest from 12 individuals (ESM Fig. 3), using CODEX (Fig. 1a and ESM Fig. 3). These proteins were selected because of their expression in human kidney based on prior data (Table 2) and relevance to kidney function or DKD pathophysiology. CD45, CD68 and CD11b staining identifies immune cells infiltrating the kidney or resident within it (Fig. 1b,d,f,i), nestin and CC motif chemokine receptor 6 (CCR6) distinguish podocytes and endothelial cells (Fig. 1c and d), and αSMA (α-smooth muscle actin), CXCR3, MUC1 and collagen IV identify blood vessels, all tubules, the distal nephron and the basement membrane, respectively (Fig. 1e,g,h). ESM Table 1 lists commercial antibody clones, sources, dilutions and the CODEX barcode and fluorophore used for each monoclonal antibody.

Table 1 Characteristics of the tissue donors

DKD class	Patient number	Age	Sex	OR date	Nephrectomy reason	Medical history	Medications	Clinical data
DM with healthy kidneys: no mesangial expansion, GS, IFTA or vascular lesions								
	1	69	M	2012	Focal metastases from low-grade B-cell lymphoma	Former smoker, hyperlipidaemia, obstructive sleep apnoea, chronic lymphocytic leukaemia	Cyclobenzaprine, ezetimibe, fenofibrate, metformin, multivitamin capsule, omeprazole, sitagliptin, vitamin D, hydrocodone/paracetamol	BP 160/85 Wt 122 eGFR 56 UA: no protein
	2	69	F	2014	RCC, clear cell	Endometrial cancer, severe obesity, cardiomyopathy, asthma, pulmonary embolus, arthritis	Albuterol, allopurinol, benazepril, calcium carbonate/vitamin D_3, carvedilol, dalteparin, docusate, gabapentin, letrozole, metformin, hydromorphone, ondansetron, letrozole, paracetamol, simvastatin, triamterene/hydrochlorothiazide, warfarin	BP 91/51 Wt 124 eGFR 46 UA: trace protein
	3	58	M	2017	RCC, chromophobe cell	Oesophageal motility disorder, adenomatous colonic polyps, rectal bleeding, diarrhoea, arthritis of knee, chronic leg and low back pain, hyperlipidaemia, insomnia, gout, lower urinary tract symptoms, diaphragmatic hernia	Allopurinol, aspirin, atorvastatin, vitamin D_3, diazepam, fentanyl, gabapentin, Hylan G-F 20, insulin lispro, lisinopril, hydrochlorothiazide, multivitamin capsule, oxycodone, pantoprazole, terazosin, verapamil	BP 128/69 Wt -125 eGFR 83–94 UA: no protein
	4	66	M	2010	RCC, clear cell	Liver problems, nephrolithiasis, heart murmur, spinal cord injury, testicular cancer	Bystolic, amlodipine, multivitamins	BP 141/81 eGFR 92
	5	48	F	2013	RCC, clear cell	Dyslipidaemia, psoriasis, DOE	Citalopram, clonazepam, hydrocodone/paracetamol, gemfibrozil, lamotrigine, pravastatin, naproxen	BP 132/80 eGFR 76
DKDIIA: mild mesangial expansion in >30% of observed mesangial areas. No GS. Mild IFTA								
	6	73	F	2011	Papillary urothelial carcinoma	Dyslipidaemia, smoker, COPD	Albuterol, hydrochlorothiazide, hyzaar, isosorbide mononitrate, levothyroxine, nexium, betapace, singulair, zetia, cymbalta, ferrous sulfate, fexofenadine, flonase, fosinopril, glibenclamide, potassium chloride, magnesium oxide, Klor-Con M10, abilify, metformin, pristiq (desvenlafaxine), meloxicam welchol, hydrocodone/paracetamol, phenazopyridine, ciprofloxacin	BP 145/59 eGFR 50
	7	61	F	2014	RCC, clear cell	CAD, severe obesity, obstructive sleep apnoea on CPAP, hiatal hernia, gout, anaemia, DDD, osteoarthritis	Albuterol, allopurinol, amlodipine, ascorbic acid, aspirin, benazepril, budesonide/formoterol, calcium, ferrous sulphate, glucosamine, chondroitin sulphate, glibenclamide, hydrochlorothiazide, metformin, multivitamin, niacin, omega-3 fatty acids (fish oil), omeprazole, oxybutynin, simvastatin	BP 126/49 Wt 114 eGFR 54–69 UA: no protein

Table 1 (continued)

DKD class	Patient number	Age	Sex	OR date	Nephrectomy reason	Medical history	Medications	Clinical data
DKDIIA–B: mild mesangial expansion in >30% of the observed mesangial areas with focal moderate mesangial expansion. No GS. Moderate IFTA								
	8	75	M	2016	RCC, clear cell	CAD, hyperlipidaemia, chronic kidney disease, severe obesity, hyperkalaemia, hyperlipidaemia	Amlodipine, chlorthalidone, diclofenac, docusate, ferrous sulphate, hydrocodone/paracetamol, metoprolol tartrate, minoxidil, simvastatin	BP 182/51 Wt 98 eGFR 38–44 UA: 30+
	9	68	F	2014	RCC, clear cell	Morbid obesity, CAD, history of breast cancer	Insulin detemir, liraglutide, anastrozole, atenolol, calcium, furosemide, levothyroxine, losartan, proton pump inhibitor, rosuvastatin, iron	BP 140/68 Wt 140 eGFR 55–63
DKDIIB: severe mesangial expansion in >30% of the observed mesangial areas. No GS. Moderate IFTA								
	10	49	F	2014	RCC, clear cell	Osteopenia, morbid obesity, gastroparesis	Aspirin, enalapril, fluoxetine, folate, gabapentin, insulin aspart, glargine, lisinopril, magnesium, metformin, methocarbamol, metoclopramide, modafinil, multivitamins, omega-3 fatty acids, propranolol, simvastatin, trazodone	BP 126/69 Wt 135 eGFR 67–78
	11	75	F	2017	RCC, clear cell	Former smoker 0.25 packs per day for 5 years (stopped smoking 17 years ago). Hyperlipidaemia, anorexia, thrombectomy	Amlodipine, aspirin, metformin, simvastatin, valsartan, docusate, hydrocodone/paracetamol, indomethacin	BP 145/71 Wt 79 eGFR 44–51 UA: trace protein
DKDIII: severe nodular GS. Severe IFTA. Severe hyaline arteriolosclerosis and at least moderate arteriosclerosis								
	12	50	M	2019	Biopsy	Dyslipidaemia, CHF, CKD	Insulin degludec, spironolactone, losartan, semaglutide, atorvastatin, bumetanide	BP 122/81 Wt 83 eGFR 22

All patients had type 2 diabetes. All patients except patient 5 had hypertension. Patients 1–7 and patient 12 were non-Hispanic white; race was not known for the remaining patients

Age is given in years, BP in mmHg, weight in kg, eGFR in mL/min per 1.73 m^2

eGFR values are not always determined pre-nephrectomy and may be confounded by the post-nephrectomy acute kidney injury and loss of nephron mass

Glibenclamide is known as glyburide in the USA and Canada

CAD, coronary artery disease; CHF, congestive heart failure; CKD, chronic kidney disease; COPD, chronic obstructive pulmonary disease; CPAP, continuous positive airway pressure; DDD, degenerative disc disease; DM, diabetes mellitus; DOE, dyspnoea on exertion; F, female; GS, glomerulosclerosis; HTN, hypertension; IFTA, interstitial fibrosis; M, male; NHW, non-Hispanic white; NK, not known; OR, operating room; RCC, renal cell carcinoma; UA, urinalysis; Wt, weight

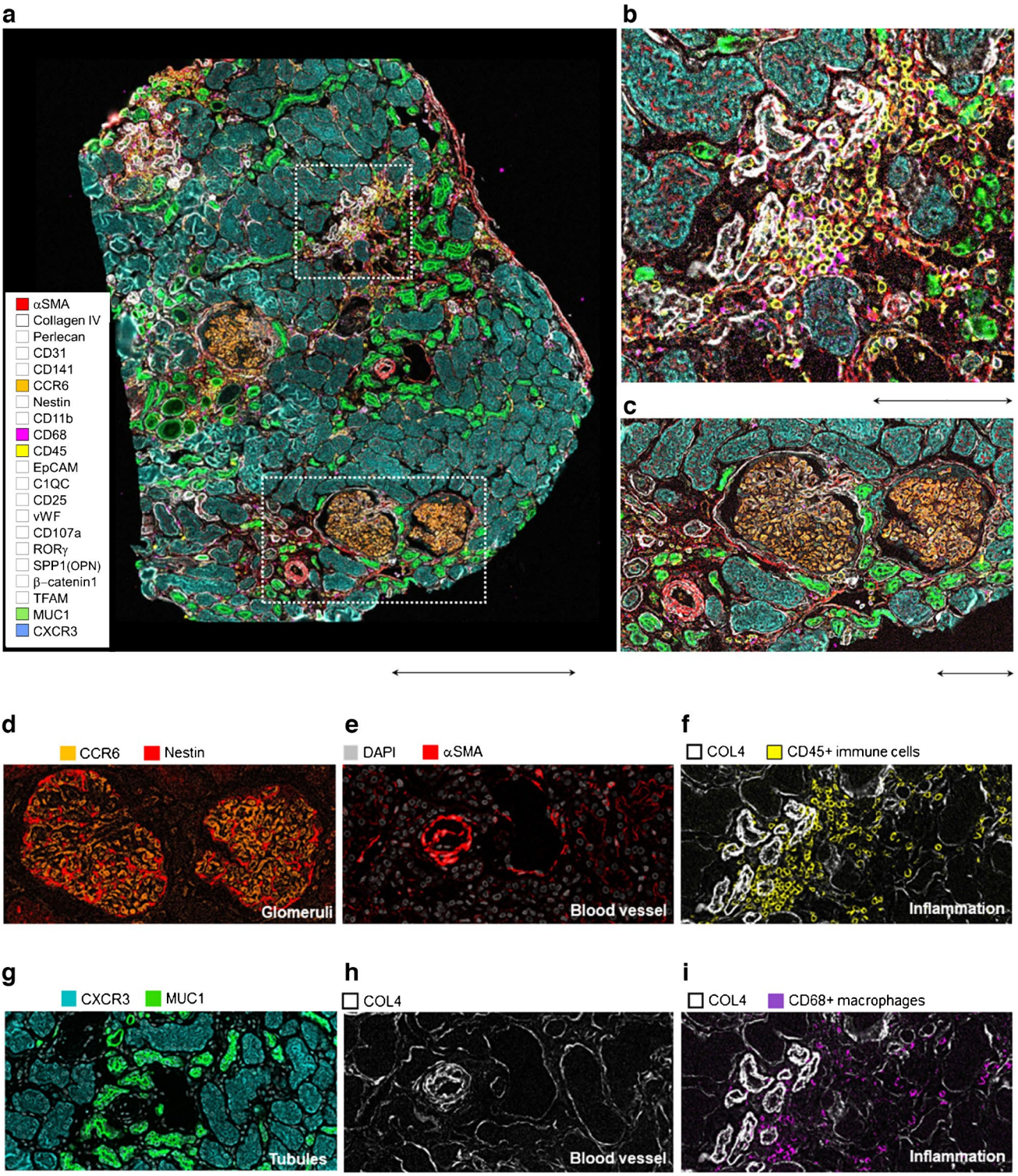

Summary of data on expression of the targeted proteins in human kidneys

Expression of the targeted proteins in our human kidney samples was compared with prior data for each protein, including the Human Protein Atlas (https://www.proteinatlas.org/) (ESM Fig. 4). For 16 of the 21 proteins, protein expression in our samples was consistent with reported expression in prior literature and/or the Human Protein Atlas. For RAR-related orphan receptor C (RORγ), there was no prior data on expression in human kidneys. Our data diverged from prior reports for nestin, CXCR3 (CD183) and osteopontin (SPP1) (Table 2).

◂**Fig. 1** Representative multiplexed immunofluorescence image showing protein expression in a kidney section with DKD. (**a**) A human kidney cortical tissue section from a patient with DKDIIB, showing the basement membrane (collagen IV, white), macrophages (CD68, purple), broad immune cells (CD45, yellow), smooth muscle and interstitial cells (αSMA, red), glomerular endothelial and peritubular capillary cells (CCR6, orange), all tubules (CXCR3, turquoise) and the distal nephron (MUC1, green). The scale bar below the image represents 500 μm. (**b**, **c**) Two zoomed-in regions from this sample show areas with increased immune cells and fibrosis (**b**), and a blood vessel and glomerular compartments (**c**). The scale bars below the images in (**b**) and (**c**) represent 100 μm. (**d**–**i**) Nestin (red), CCR6 (orange) (**d**), αSMA (red) (**e**), CD45 (yellow) (**f**), CXCR3 (turquoise), MUC1 (green) (**g**), collagen IV (white) (**h**) and CD68 (purple) (**i**) highlight podocytes, GEC, blood vessels, inflammatory cells, all tubules, the distal nephron, basement membrane and macrophages, respectively. COL4, collagen IV; C1QC, complement C1q C chain; EpCAM, epithelial cell adhesion molecule; MUC1, mucin 1, also known as CD227; SPP1, secreted phosphoprotein 1, also known as osteopontin (OPN); TFAM, transcription factor A, mitochondrial; vWF, von Willebrand factor

Identification of the known cell types and tissue compartments in the kidney

Unsupervised clustering from the 21-protein expression profiles was used to assign cell types to all segmented cells, leading to identification of 11 clusters. The clusters were classified into 11 distinct cell populations based on the bulk expression profiles of each cluster (Fig. 2a,b). The identified cell populations were proximal tubules ($CXCR3^{++}$/$MUC1^{-}$), the distal nephron ($CXCR3^{lo}$/$MUC1^{+}$), glomerular endothelial cells (GEC) and peritubular capillaries ($CCR6^{+}$/$CD31^{+}$), vascular endothelial cells ($CCR6^{lo}$/$CD31^{+}$), vascular smooth muscle cells (αSMA^{+}), glomerular podocytes ($nestin^{+}$), macrophages ($CD68^{+}$), cells of the myeloid lineage ($CD11b^{+}$) and other immune cells ($CD45^{+}$/$CD68^{-}$/CD11b). Segments that were positive for collagen IV/heparan sulphate proteoglycan (HSPG) were categorised as 'basement membrane'. Cells exhibiting low expression of all proteins were categorised as 'low-expressing' cells.

Because the initial cell classification results were generated algorithmically and without supervision, we validated these classification results using several methods: first, we verified that each identified cell population expressed the expected combination of proteins (Fig. 2a,b). Second, we determined that minimal batch effects from unsupervised clustering were observed (ESM Fig. 5). Third, we confirmed that the Voronoi representations of the samples showed the expected spatial localisation of the identified cell populations (Fig. 2c). Finally, we confirmed the results by overlaying cell annotations with CODEX image channels of cell-type specific biomarkers (Fig. 2d).

Global and compartment-wise changes in protein expression from health to DKDIII

We then used unsupervised clustering in entire sections to quantitatively compare the cellular composition of the kidney samples across DKD classes (Fig. 3a). Transition from diabetes mellitus to progressive DKD was associated with an increase in inflammatory cells (macrophages, inflammatory cells of the myeloid lineage and $CD68^{-}$/$Cd11b^{-}$/$CD45^{+}$ cells), as well as decrease in proximal tubular cells (Fig. 3a). In addition to global cell-type identification, we used unsupervised clustering of protein expression to determine cell-type frequencies in six distinct tissue compartments (glomeruli, blood vessels, distal tubules, all tubules, collagen IV^{+} areas, and the interstitium), determined as described in Methods (Fig. 3b). The glomerular compartment showed a decrease in podocytes ($nestin^{+}$ cells) and $CCR6^{+}$/$CD31^{+}$ GEC with progression from diabetes mellitus to DKDIII, and an increase in αSMA^{+} cells and the collagen IV^{+}/$HSPG^{+}$ basement membrane. The proximal tubule compartment showed a decrease in proximal tubular cells and an increase in $CD45^{+}$ immune cells and macrophages, while the cellular composition of the distal nephron compartment, marked by MUC1 expression, was grossly unchanged. Blood vessels showed a reduction in αSMA^{+} cells and a mild reduction in $CCR6^{lo}$/$CD31^{+}$ endothelial cells, and the interstitium had a subtle decrease in $CCR6^{lo}$/$CD31^{+}$ endothelial cells and an increase in $CD45^{+}$ immune cells and low-expressing interstitial cells. Finally, the basement membrane showed an increase in collagen IV^{+}/$HSPG^{+}$ regions and $CD45^{+}$ inflammatory cells (Fig. 3b).

Hierarchical clustering based on cell frequencies in the cortical tissue sections reiterated the higher abundance of immune cells, collagen IV^{+}/$HSPG^{+}$ and αSMA^{+} cells in DKD tissues vs those from participants with diabetes mellitus and healthy kidneys (Fig. 3c, red-bordered box), while sections from the participants with diabetes mellitus and healthy kidneys had more cells from proximal tubules and the distal nephron, as well as glomerular $nestin^{+}$ and $CCR6^{+}$ cells (Fig. 3c, green-bordered box). Individuals within each DKD class showed significant variation in these findings (Fig. 3c). Overall, however, the increase in inflammatory cells was statistically significant and continuous from the participants with diabetes mellitus and healthy kidneys to those with DKDIII (Fig. 3d,e). The increases in these inflammatory cell groups retained significance after Bonferroni-adjusted correction for multiple testing, even when the DKDIII sample was excluded (ESM Fig. 6a,b).

Visual examination of protein changes from health to DKDIII

Visual examination reiterated the data obtained from bioinformatic analysis in the preceding sections, i.e. there was an increase in fibrosis and inflammatory cells with

Table 2 Summary of data on expression of the targeted proteins in human kidneys

Protein	Location of expression based on prior data	Human Protein Atlas	Our data	Conclusion for expression in kidneys of people with DM
αSMA	Blood vessels, interstitium [9, 10]	3 of 3 mAbs: interstitial, blood vessels 1 of 3 mAbs: some proximal tubular stain	Blood vessels, interstitium	Blood vessels, interstitium
C1QC	Only for C1Q, not C1QC: Interstitial/immune cells [11] None [12–14] Glomeruli, arterioles [15]	All tubules with variations	Proximal tubules > distal nephron 2	Proximal tubules > distal nephron 2
CCR6 (CD196)	GEC and PTC [16]	GEC, PTC Tubules in some individuals with some of the mAbs	GEC, PTC	GEC, PTC
CD11b	Monocytes and granulocytes [17, 18]	Individual tissue resident cells Low level expression in proximal tubules	Monocytes and granulocytes	Monocytes and granulocytes
CD31	Glomeruli, venules, arteries > capillaries [19]	Glomeruli, venules, capillaries	Glomeruli, venules, arteries, capillaries	Glomeruli, venules, arteries capillaries
CD45	All haematopoietic cells except erythrocytes [20]	All haematopoietic cells except erythrocytes	All haematopoietic cells except erythrocytes	All haematopoietic cells except erythrocytes
CD68	Monocytes [11] and macrophages [21]	Not detected (individual cells visible, however)	Monocytes and granulocytes	Monocytes and granulocytes
Collagen IV	Mesangial matrix (4A1), Bowman's capsule (4A1, 4A5), GBM (4A3, 4A5), tubular BM (4A1) [22]	Mesangial matrix, Bowman's capsule, tubular BM (4A1, 2) Glomerular mesangial cells, proximal tubules (4A3)	Mesangial matrix, GBM, Bowman's capsule, tubular BM	Mesangial matrix, GBM, Bowman's capsule, tubular BM
β-Catenin1	Proximal tubules, thin and thick ascending limbs, distal convoluted tubules, collecting duct [23]	Tubular epithelia	All tubular epithelia	All tubular epithelia
CXCR3 (CD183)	mRNA expressed in micro-dissected human proximal tubules (and rat immunohistochemistry) [24] None [25–27] VSMC [28, 29] Endothelial cells [29] Afferent arteriole, low-level glomerular cells [28]	One mAb used: no expression detected	Proximal and distal convoluted tubules, collecting ducts	
EpCAM	Distal convoluted tubule ≈ loop of Henle > collecting duct [30] Distal convoluted tubule > collecting duct [31] Collecting duct > distal convoluted tubule [32] Cortical collecting duct [33]	Collecting duct >> distal tubules	Collecting duct >> distal tubules	Collecting duct >> distal tubules

Table 2 (continued)

Protein	Location of expression based on prior data	Human Protein Atlas	Our data	Conclusion for expression in kidneys of people with DM
HSPG2 (perlecan)	Arterioles [34] Arteries [35] Tubular BM [34, 35] GBM [35]	Arteries, arterioles, glomerular vascular pole (3 of 4 mAbs) Low–medium ubiquitous expression (3 of 4 mAbs)	Blood vessels, tubular BM, weak glomerular BM and mesangial matrix	Blood vessels, tubular BM, weak glomerular BM
LAMP1 (CD107a)	Ubiquitous [36]	Ubiquitous	Ubiquitous	Ubiquitous
TFAM	All tubules, none in gloms [37]	All tubules	All tubules	All tubules
MUC1 (CD227)	Distal convoluted tubule, collecting duct [38, 39]	Distal convoluted tubule, collecting duct	Distal convoluted tubule, collecting duct	Distal convoluted tubule, collecting duct
Nestin	Glomerular podocytes [40, 41]	Glomerular podocytes, peritubular capillaries, endothelium, low level in proximal tubules (1 of 4 mAbs)	Podocytes, proximal tubules, small medullary vessels	Podocytes, small medullary vessels
RORγ	Isoform 1 (RORγ1) mRNA is expressed in kidneys [42–44]. The mAb used recognises both isoforms but is commercially defined as identifying RORγt because that is the only isoform in immune cells. No data on protein	No expression	Ubiquitous nuclear expression	Ubiquitous nuclear expression
SPP1 (osteopontin)	Thick ascending loop of Henle [45] Distal convoluted tubules [45–47] Collecting duct [46, 47] Some proximal tubules [46]	Proximal and distal convoluted tubules	Proximal and distal convoluted tubules, collecting ducts	
TM (CD141)	Weak and segmental in glomerular vessels, stronger in peritubular capillaries [48] Vascular pole of glomerulus, reduced in glomeruli of people with DM [49] Glomerular vascular pole, peritubular capillaries [50]	Peritubular capillaries, glomerular vascular pole, blood vessels	Peritubular capillaries, blood vessels	Peritubular capillaries, blood vessels. Staining in glomerular vascular pole reduced due to DM in our samples
vWF	Venules, arterioles, capillaries [19] Unclear whether it is expressed in glomeruli (yes [51]; no [19])	Reported as not detected, but is visible in venules and arterioles	High-intensity staining in venules, arterioles and arteries. Low-grade staining in parenchyma	Venules, arterioles, capillaries

αSMA, alpha smooth muscle actin; mAb, monoclonal antibody; C1QC, complement component 1QC; CCR6, CC motif chemokine receptor 6; PTC, peritubular capillary; GBM, glomerular basement membrane; BM, basement membrane; CXCR3, CXC motif chemokine receptor 3; VSMC, vascular smooth muscle cell; LAMP1, lysosomal associated protein 1; TFAM, transcription factor A, mitochondrial; TM, thrombomodulin; vWF, von Willebrand Factor

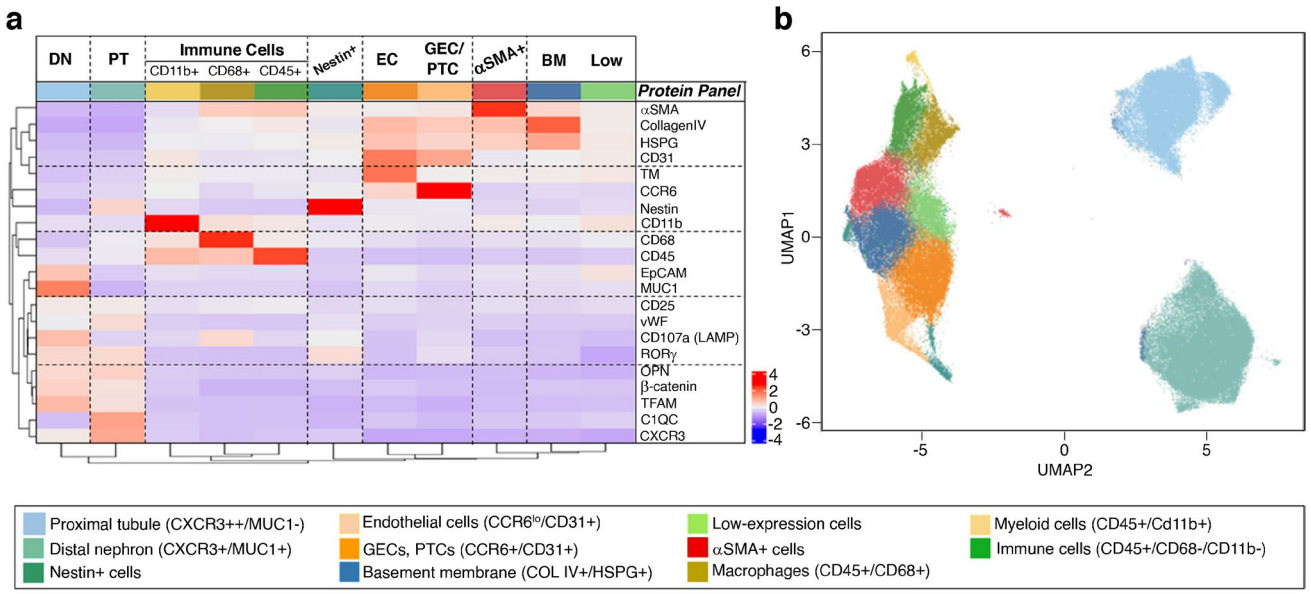

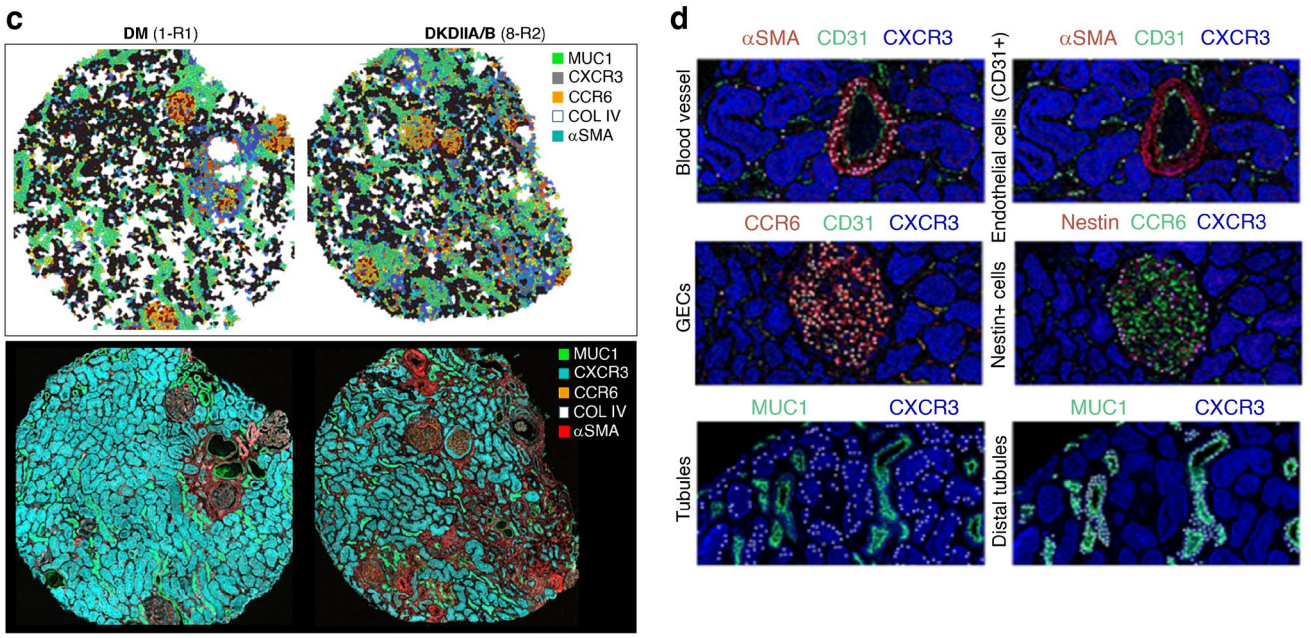

Fig. 2 Classification of kidney cell types and tissue compartments. (**a**) Heatmap of protein expression by phenotype showing unique expression profiles for the cell populations identified in this study, as well as the low-expressing cells. (**b**) A uniform manifold approximation and projection (UMAP) representation of all cells in the study, coloured by cell type. (**c**) A Voronoi representation of cortical sections from a healthy kidney sample and one from a donor with DKDIIA–B, coloured by cell type (top panels), compared with expression of compartment-identifying proteins in the same tissue sections (bottom panels). 'R' denotes the region number, e.g. 1-R1 for region (section) 1 from individual 1. (**d**) Cell types identified from unsupervised clustering were validated by overlaying cell annotations (white dots) with cell type-specific marker protein channels. BM, bone marrow; COLIV, collagen IV; C1QC, complement C1q C chain; DM, diabetes mellitus; DN, distal nephron; EC, endothelial cell; EpCAM, epithelial cell adhesion molecule; LAMP, lysosome-associated membrane protein; MUC1, mucin 1, also known as CD227; OPN, osteopontin; PT, proximal tubule; PTC, peritubular capillary endothelial cell; TFAM, transcription factor A, mitochondrial; TM, thrombomodulin; vWF, von Willebrand factor

DKD progression (Fig. 4a) and a progressive loss of proteins marking tubular and glomerular compartments (Fig. 4b). Also notable was a difference in the trajectory of change in expression of the segment marker proteins. For example, MUC1 was expressed through DKDIII, while CCR6 and CXCR3 expression was reduced or lost in earlier classes. In addition, co-staining for collagen IV, CD45 and CD68 showed that the increases in inflammatory cells

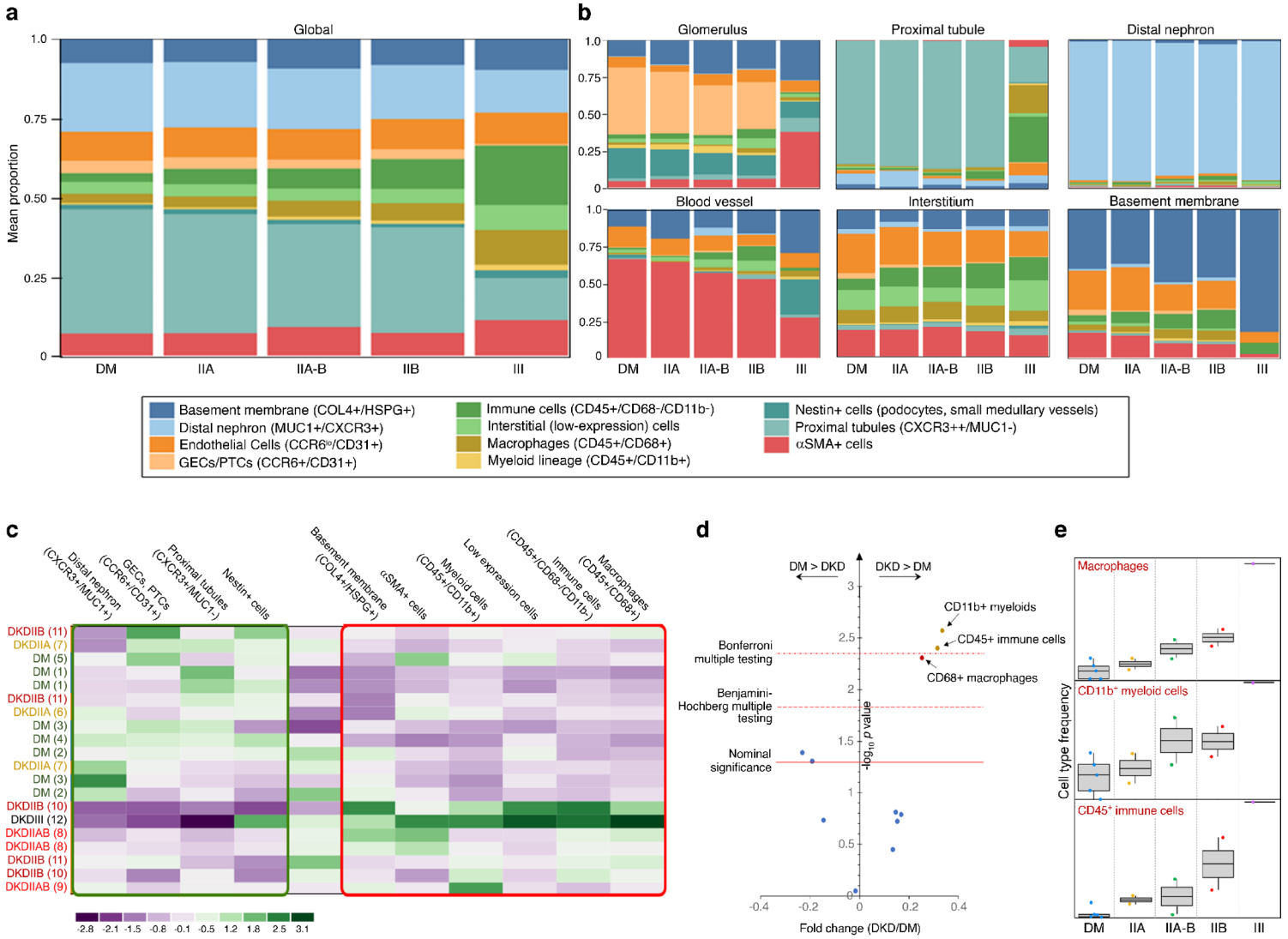

Fig. 3 Global and compartment-wise changes in cell-type proportions and protein expression from diabetes to DKD. (**a**) Bar graph of cell frequency showing global change in fraction of cell types when the data are aggregated by DKD class. (**b**) Compartment-wise change in the distribution of cellular composition in glomeruli, proximal tubules, distal nephron, blood vessels, interstitium and basement membrane with DKD progression. Sections of the bars from top to bottom correspond to the cell types/segments depicted in the legend from left to right. (**c**) Hierarchical clustering based on cell-type frequency in the cortical tissue sections, where the columns represent cell types identified from unsupervised clustering, and the rows represent individual tissue sections. Cell-type frequencies are represented as *z* scores per column (cell type) and values are normalised by column. The heatmap shows coarse segregation of cortical sections from people with diabetes mellitus and DKD, but with overlap between classes. (**d**) Volcano plot of cell-type frequency showing enrichment of all inflammatory cell types in DKD, compared with healthy kidneys, with significant increases in $CD11b^+$ and $CD45^+$ cells after Bonferroni adjustment for multiple testing. (**e**) Boxplots of cell-type frequency, grouped by DKD class, showing that the increase in immune cells is continuous from diabetes mellitus to DKDIII. Each dot represents a single individual within each DKD class. COL4, collagen IV; DM, diabetes mellitus; PTC, peritubular capillary endothelial cell

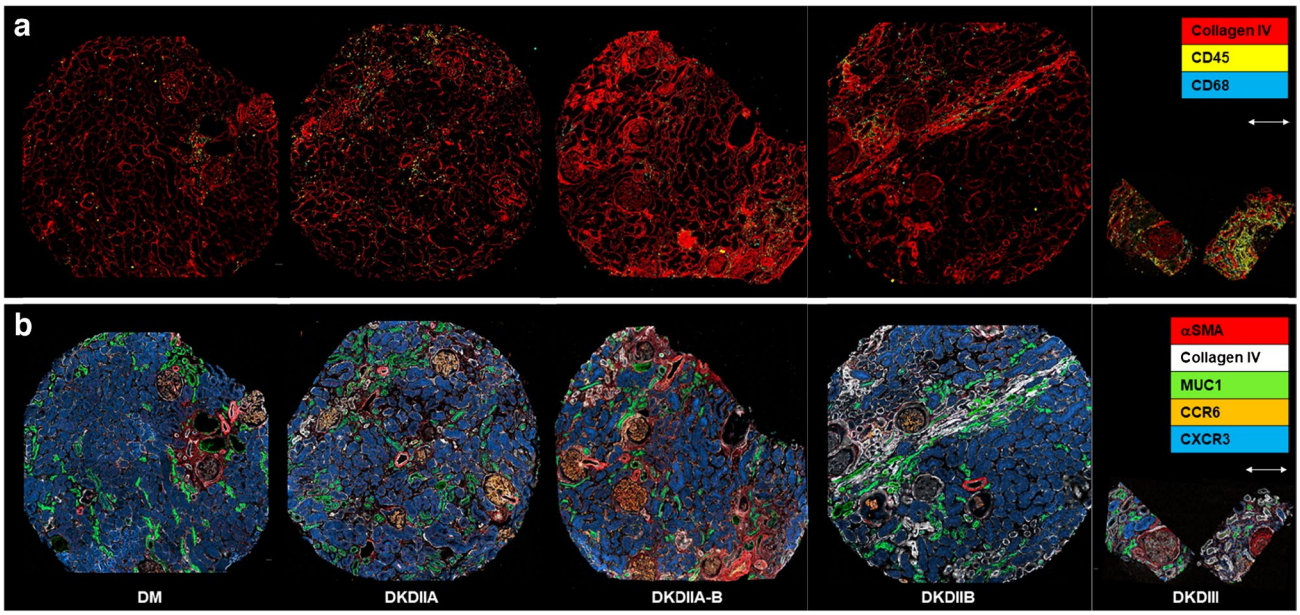

Fig. 4 Representative multiplex immunofluorescence images showing protein expression across the spectrum from healthy kidneys to progressive DKD. (**a**) Staining for basement membrane (collagen IV, red), broad inflammatory cells ($CD45^+$, yellow) and macrophages ($CD68^+$, blue) shows that disease progression, manifested by basement membrane (collagen IV) thickening, is patchy. In addition, inflammatory cells, including macrophages, coincide with areas of greater collagen IV deposition. (**b**) The expression of compartment-identifying proteins (CXCR3, turquoise; CCR6, orange; MUC1, green; collagen IV, white; αSMA, red) differs between DKD classes. The scale bars represents 250 μm. DM, diabetes mellitus

and fibrosis co-localised in the same areas, and that the extent of tissue injury, as shown by increases in collagen IV deposition and inflammatory cells, was regional and patchy (Fig. 4a,b).

DKD is patchy: quantifying section- and patient-level heterogeneity in cellular composition and protein expression

Our visual observations suggested that DKD severity was regional and progressed in patches (Figs 1 and 4). We used several informatic tools to quantitatively assess this visual observation (Fig. 5). First, we mapped the correlation between histopathological features/sub-regions of a single tissue to the overall DKD class assigned to the individual. Sub-regions with varying DKD severity were manually outlined in a tissue section from a patient with DKDIIB (individual 10) by a pathologist. Based on histopathological severity, these areas were labelled as healthy (histologically intact), moderately fibrotic or severely fibrotic (Fig. 5a). The sub-regions were then projected as individual specimens onto the principal component space defined by the 23 tissue sections, classified as DKDIIA to III. Within this space, healthy, moderately fibrotic and severely fibrotic sub-regions from one individual tissue section co-localised with tissue sections from healthy kidneys, intermediate DKD (IIA to IIA–B) and severe DKD. Thus, a single tissue section from one individual displayed wide pathological variability, running the gamut from healthy kidneys to DKDIII (Fig. 5b). Second, we examined intra- and inter-individual variability in expression of the CCR6 protein, which marks the glomerular compartment. This compartment was selected because glomeruli were manually outlined and glomerular sclerosis is a known feature of DKD progression. Normalised CCR6 expression in GEC was calculated in outlined glomeruli from two individuals with DKDIIB (individuals 10 and 11). We observed substantial variability in normalised glomerular CCR6 expression both within an individual participant (e.g. individual 10, Fig. 5c,d) and between the two individuals with DKDIIB (individuals 10 and 11, Fig. 5c,d).

Hierarchical clustering of individual cortical tissue sections based on adjacency between cell types

Heatmap dendrograms of cell–cell adjacency were used to segregate histologically normal and DKD kidney tissues. Consistent with the observed changes in cell types, DKD tissues showed an increase in cell–cell adjacencies, including inflammatory cells, αSMA^+ cells and the basement membrane (Fig. 6a, red-bordered box). Also consistently,

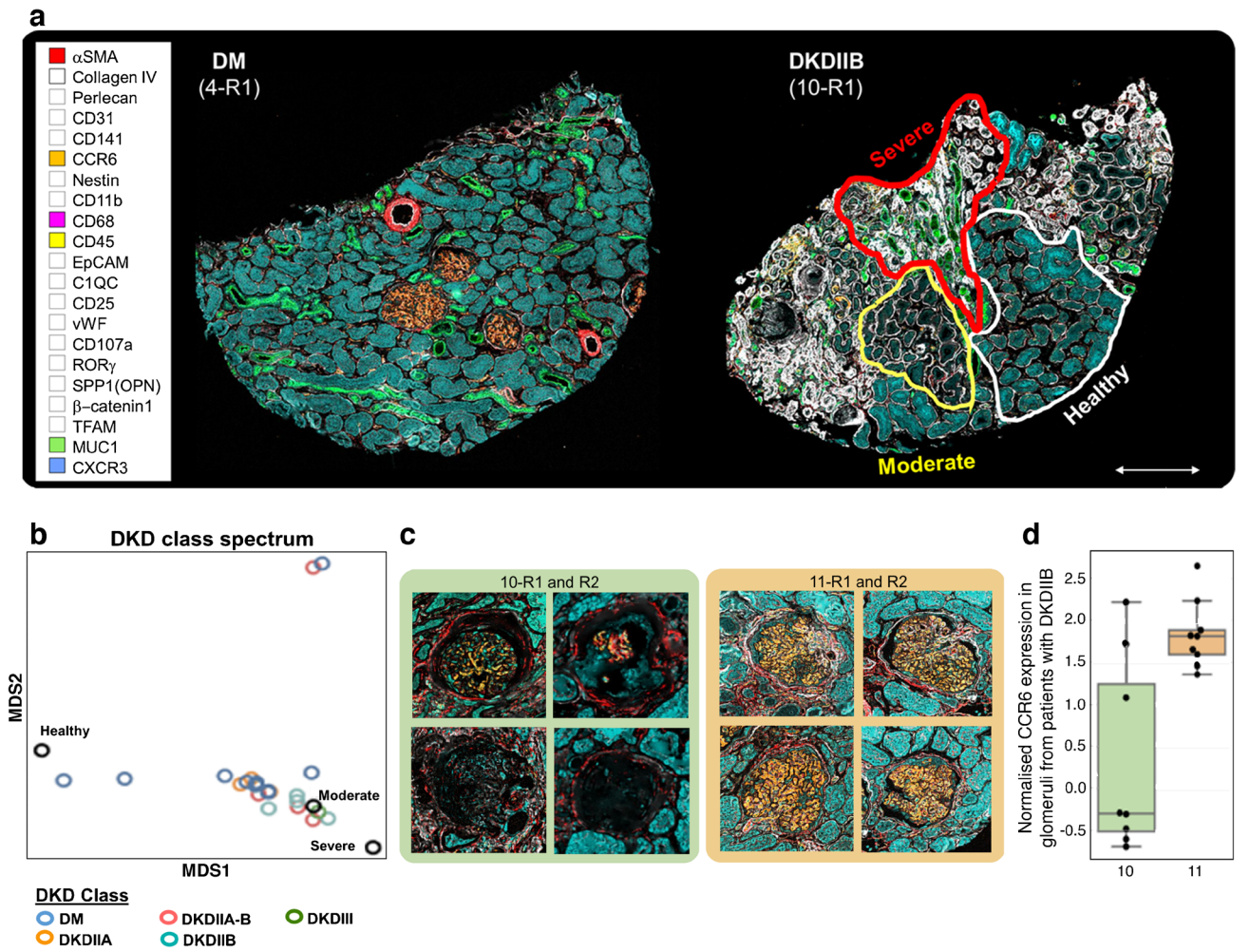

Fig. 5 DKD is patchy. (**a**) Representative multiplex immunofluorescence images showing DKD heterogeneity (sample 10-R1, right) in terms of alteration of protein expression compared with normal tissue (sample 4-R1, left); 'R' denotes the region number, e.g. 4-R1 for region (section) 1 from individual 4; scale bar, 250 μm. Regions with variable DKD severity are manually outlined. (**b**) Multidimensional scaling (MDS) plot of 20 cortical sections (omitting the three medullary sections), coloured by disease class, as well as the three manually outlined sub-regions. (**c**) Representative images of manually outlined glomeruli in two DKDIIB sections from patients 10 and 11. (**d**) Boxplot comparing normalised CCR6 expression in glomeruli from the two sections. Each dot represents CCR6 expression in a single outlined glomerulus. C1QC, complement C1q C chain; DM, diabetes mellitus; EpCAM, epithelial cell adhesion molecule; SPP1, secreted phosphoprotein 1, also known as osteopontin (OPN); TFAM, transcription factor A, mitochondrial; vWF, von Willebrand factor

histologically normal tissues showed more frequent cell–cell adjacencies involving cells of the proximal and distal nephron, as well as nestin$^+$ and GEC (Fig. 6a, green-bordered box). As for other data, there was marked variation in these observations between individuals in the same DKD class. Nonetheless, the increase in proximity between CD45$^+$ immune cells and cells of the distal nephron, proximal tubules and αSMA$^+$ cells was robust to Bonferroni adjustment for multiple testing (Fig. 6a,b). These cell–cell proximities remained significant and robust to Bonferroni-adjusted correction for multiple testing even when the DKDIII sample was excluded (ESM Fig. 7a,b).

Discussion

We developed Spatial TissuE Proteomics (STEP), a pipeline that combines curated human kidney tissues, a multiplexed immunofluorescence platform [8] and powerful analysis tools to compare expression of 21 proteins in human kidneys from people with diabetes and histologically normal kidneys (10 sections, five individuals) to those with DKD classes IIA to III (13 sections, seven individuals). Expression of these 21 proteins identified 11 functionally relevant kidney compartments or cell types. The data from this spatial proteomics pipeline reiterated the increases in the inflammatory cells

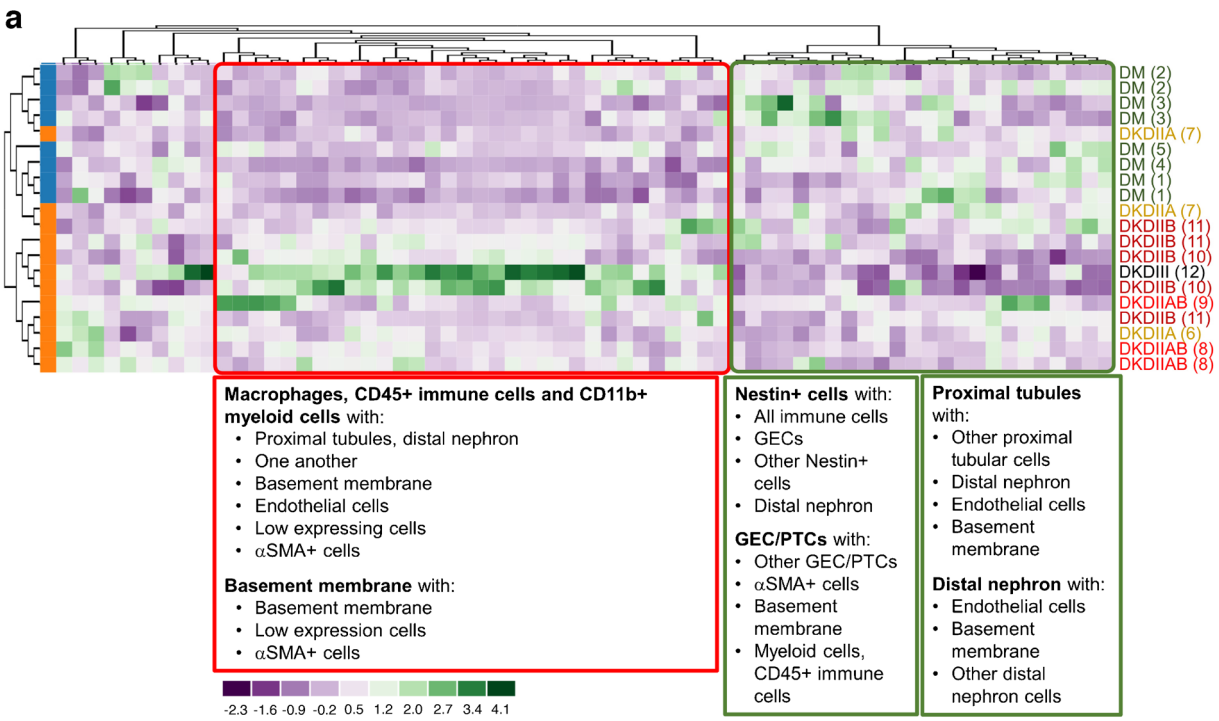

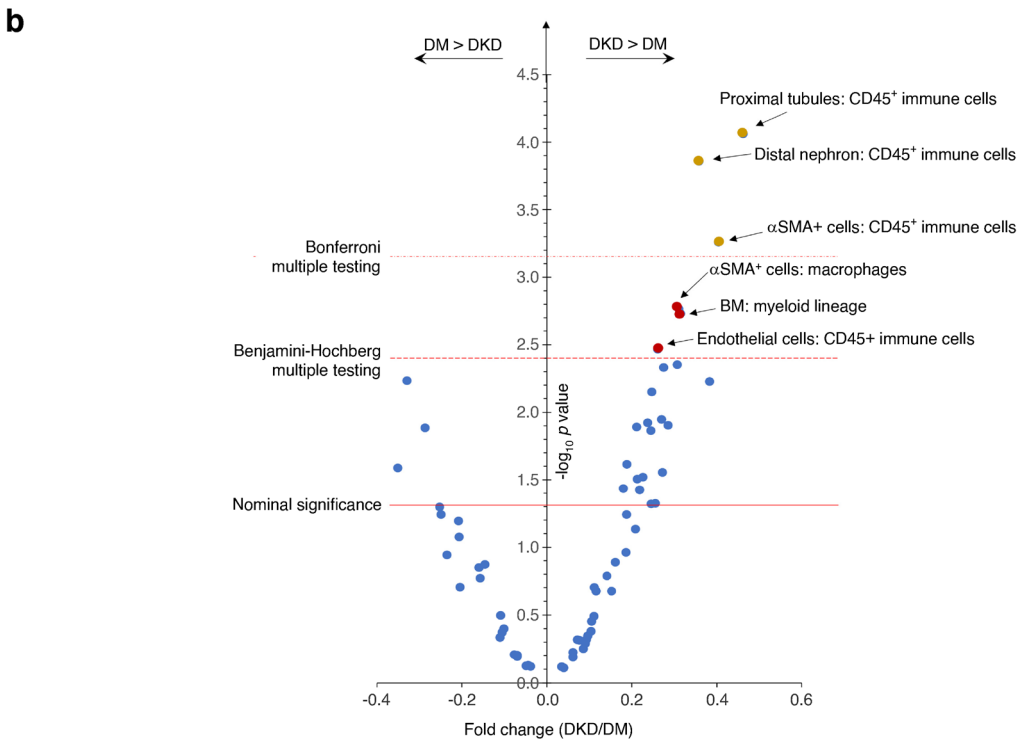

Fig. 6 Cell–cell proximities in diabetes mellitus vs DKDIIA–III. Hierarchical clustering of cortical tissue sections based on cell–cell adjacency between cell types. (**a**) Heatmap dendrogram of cell–cell adjacency, segregating healthy kidneys from DKD. Cell–cell adjacencies also show significant inter-individual heterogeneity within each DKD class. Values are normalised per column using z scores; data are clustered by rows. (**b**) Volcano plot of cell adjacencies showing enrichment of proximity between immune cells, tubular cells (proximal and distal) and αSMA$^+$ cells in DKD, compared with healthy kidneys, after Bonferroni adjustment for multiple testing. BM, basement membrane; DM, diabetes mellitus; PTC, peritubular capillary endothelial cell

and collagen IV, as well as the resultant reduction of native proteins marking proximal tubules and glomeruli, in people with DKD. In addition, the results highlighted several new datapoints: first, the increase in inflammatory cells and fibrosis was strictly co-localised, suggesting concomitant occurrence rather than fibrosis occurring after inflammation, as had been expected from animal studies. Second, these data suggested that the expression of proteins marking different nephron segments followed distinct trajectories: e.g. CCR6 reduction occurred by stage IIB, while MUC1 expression persisted through to stage III. Finally, spatial proteomics showed a marked patchiness in DKD severity, revealing sizeable intra- and inter-individual variability in the molecular pathology of disease progression in the kidney tissue. This finding underscores the limitations of kidney biopsies in providing whole-kidney assessment of DKD severity. Clustering based on cell type or cell–cell proximities confirmed the increases in inflammatory cells in DKD, and, in addition, showed proximity between inflammatory cells and proximal and distal tubular cells, as well as those expressing αSMA, with statistical significance, that was robust to adjustment for multiple testing even in this limited sample set. These findings displayed the power of spatial proteomics in identifying significant changes in cell type and cell–cell interactions.

First, this report shows that a relatively small (21-protein) panel may be used to segregate kidneys into 11 clusters, corresponding to several of the known and functionally important kidney compartments and cell types. Each cluster is identifiable by its specific expression profile for the 21 proteins, including expression of marker proteins (e.g. MUC1, identifying the distal nephron). Within each cluster/compartment, quantification of all 21 proteins allowed characterisation of disease-associated alterations in these proteins from individuals with diabetes mellitus but no kidney disease to those with DKDIII. Comparing cell types in cortical sections from individuals with diabetes mellitus but no kidney disease to those with DKD reiterated the themes of co-localised fibrosis and inflammatory cell increase, as well as a reduction in proteins marking proximal tubular and glomerular compartments. Compartment-wise examination of these changes showed a reduction in proteins specific to the compartment, but with trajectories that were distinct for each protein and compartment. For example, $CCR6^+$ and $nestin^+$ cells were reduced in glomeruli with DKD progression, and distal tubules showed little to no change in MUC1 staining. In addition, examining compartment-specific protein alterations revealed compartment-specific nuances in DKD-associated changes in protein expression. For example, with DKD progression, αSMA^+ cells were increased in glomeruli but reduced in blood vessels, suggesting an alteration not only in the quantity but also the site of αSMA expression, away from its normal cell types in vessel walls and towards abnormal sites such as glomeruli. This finding emphasises the importance of using histological features to manually outline compartments because the compartment/cell-type-specific marker proteins may no longer be expressed with DKD progression, or their pattern of expression may change.

Second, we present data on expression of these 21 proteins in human kidneys. To draw firm conclusions on expression of the targeted proteins, our data were compared with all existing expression data (to our knowledge) for each protein, and critically analysed (Table 2). We included all available data on potential sources of pre-analytic variability for our samples, including donor characteristics (demographic, clinical, etc.), tissue source and processing (Table 1), as well as the antibodies used (ESM Table 1), to enable comparisons with studies by other authors. For 16 of the 21 proteins, the data reported here were supported by prior literature, allowing determination of the sites of protein expression in human kidneys from people with diabetes, with or without DKD. For four of identified proteins (CXCR3, osteopontin, nestin and RORγ), our data either varied from prior data, or there was no prior data available or no consensus on expression of the protein in human kidneys. For example, while we used CXCR3 as a pan-tubular marker, its expression has not previously been reported in tubules. Examining CXCR3 expression in healthy tumour nephrectomies from people without diabetes also showed pan-tubular CXCR3 expression (ESM Fig. 8), demonstrating that this pattern was not related to diabetes and was most likely due to presence of the tumour, as suggested by prior literature (see ESM Discussion).

Third, cell-frequency and neighbourhood (cell–cell adjacency) analyses provided other examples of how bioinformatic analyses of spatial proteomics can shed light on disease mechanisms. As proof of principle, we present an example of these analyses, highlighting the increase in inflammatory cells and their proximity to the cells of the nephron in DKD tissues compared with healthy kidneys from people with diabetes. Interestingly, heterogeneity was again in evidence in both cell-frequency and neighbourhood analyses.

Fourth, we observed striking patchiness in DKD severity. These variations may be due to sampling bias, which may cause the DKD class in the multiplex immunofluorescence-stained section to differ from that of the section used for pathological staging (a few microns apart). In addition, the complexity of the underlying DKD mechanisms may lead to intra-individual heterogeneity in protein expression within one tissue section or between multiple tissue sections, or between individuals within one DKD class. This marked intra- and inter-individual variability was evaluated by visual examination and quantified using bioinformatic analyses. While use of visual examination is clearly limiting in terms of the substantial number of sections needed to overcome biological variability in human tissues, it was the impetus and reason for quantitative assessment of this variability

using the more powerful and far-reaching bioinformatic tools. In this context, juxtaposition of one kidney biopsy core with tissue sections obtained from partial nephrectomy (Fig. 4) stressed the scale and probable impact of this limitation in tissue sampling on our clinical assessment of DKD severity in entire kidneys.

Finally, we describe a human kidney proteomics pipeline, comprising a human kidney biorepository, a multiplex immunofluorescence platform and the combined expertise in clinical nephrology, renal pathology, histotechnology, epidemiology, biostatistics and bioinformatics required for generation of reliable spatial proteomics data in human kidneys. This tissue repository includes the required controls (e.g. histologically intact kidney tissue from donors with diabetes but not DKD) as well as tissues from donors with DKD classes I to III, classified by an experienced renal pathologist. Tissues from donors with DKD classes IV and V were not included because the severity of scarring in these classes significantly reduces their data content.

This study adds to the exciting body of work using spatial proteomics in human kidneys, and expands our molecular companion to DKD pathological classification. Not surprisingly, this initial study has generated several new questions to be addressed in subsequent studies. For example, performing protein staining in the same section as used for pathological DKD classification would help to pair protein expression and tissue pathology more closely, by reducing the observed variation in DKD class from section to section of the same tissue. In addition, while tissues from people with diabetes are the appropriate controls for those with DKD, a full understanding of changes in protein expression requires inclusion of kidney tissues from people without diabetes or kidney disease, as well as those with non-diabetic CKD. Furthermore, DKD almost always co-exists with other comorbidities, such as hypertension or dyslipidaemia. Therefore, another set of critical controls are histologically normal tissue sections from people with these comorbidities but not diabetes. The most significant limitation of this study, shared by many spatial omics data in human DKD, is reliance on tumour nephrectomies as the tissue source. Unfortunately, however, no current tissue source is free of caveats: DKD clinical biopsies are usually from atypical cases, and research-grade biopsies usually come from highly motivated participants from higher socioeconomic classes, although the disease burden is heaviest in patients in the lowest socioeconomic classes, who are least likely to participate. The key may be to recognise, and remedy, these caveats, rather than search for the perfect human tissue source, which, even if possible, would significantly restrict the number of available samples. For example, observations that are replicated in tissues from a variety of sources are more reliable because differing biases from a variety of sources would be less likely to point in the same direction: e.g. with DKD progression, we observed a monotonic increase in inflammatory cells in DKDIIA to IIB kidneys from tumour nephrectomies, which was continuous with that observed in the DKDIII tissue from a clinical biopsy (individual 12). Another caveat to the use of tumour nephrectomies as in the current study, albeit one that can be remedied, is that data on two cardinal clinical parameters of kidney function (eGFR and urine albumin or protein) are often obtained after, not before, nephrectomy.

As with any other study in human participants, strength is in numbers: of individuals, of tissue sections per individual and of proteins assessed. This and other spatial proteomics studies must expand to large and diverse patient populations (including more individuals and more tissue sections per individual) so that the observed molecular associations can be statistically adjusted for potential confounding variables. This throughput is currently limited by the scarcity and difficulty of access to tissue samples, and the cost of acquiring and running the current spatial proteomics platforms, a shortcoming that will hopefully improve with time. One example of such improvements is the high-volume pipeline of available tissues and use of a flexible, expandable multiplex immunofluorescence platform, as described here.

In conclusion, we present a spatially resolved proteomics dataset comparing expression of 21 proteins in 23 tissue sections from five individuals with diabetes and histologically normal kidneys vs seven individuals with DKDIIA to III. This work adds to current efforts targeting greater understanding of the changes in protein expression and cell composition in human DKD.

Supplementary Information The online version of this article (https://doi.org/10.1007/s00125-024-06210-8) contains peer-reviewed but unedited supplementary material.

Acknowledgements Specimens and services were provided by the GU001 protocol and the UC Davis Shared Biorepository Resource, as well as the UC Davis Department of Pathology and Laboratory Medicine. The authors owe a debt of gratitude to I. Feldman, R. Clarke, A. G. Proffitt and R. Sacchi (UC Davis Shared Biorepository Resource, Davis, CA, USA) for their solid knowledge base, peerless expertise and work ethics, meticulous and productive work and incredible collaborative spirit.

Data availability All data, code and materials used in the analysis are present in the paper or the ESM and are also available via the Enable Medicine portal (https://app.enablemedicine.com/portal/).

Funding This work was supported by Richard A. and Nora Eccles Foundation award A20011, the Richard A. and Nora Eccles Harrison Endowed Chair in Diabetes Research and the Depner Endowed Chair in Nephrology Research (MA). The UC Davis Shared Biorepository Resource is funded by a UC Davis Comprehensive Cancer Center support grant awarded by the National Cancer Institute (NCI P30CA093373).

Authors' relationships and activities The authors declare that there are no relationships or activities that might bias, or be perceived to bias, their work.

Contribution statement AK performed the bulk of the data analyses and contributed to writing the manuscript and generating figures. MM contributed to data analyses, generating figures and writing the methods section of the manuscript. RP performed the bulk of the multiplex immunofluorescence experiments. HA, AET and AL contributed to data analysis and interpretation, and writing the manuscript. ZW contributed to data analysis and writing the methods section of the manuscript. HBD'A contributed to the biomarker panel optimisation and design. DN, HKB, CRV and AR contributed to the image analysis. HKB, CRV, LNL and AR contributed to the data generation and literature review. AR contributed to the literature review and image analysis. NW and SSH contributed to study idea and image analysis. MD'E contributed to the acquisition of data and drafting of the manuscript. K-YJ reviewed all tissues, determined DKD classes, contributed to the idea and study design and critically reviewed the data. ATM contributed to the idea and study design, directed the performance of studies and bioinformatic analysis of the data and generated figures. MA serves as the guarantor for this study, accepting primary responsibility for the integrity of this work as a whole and the conduct of the study. She had access to the data and controlled the decision to publish. She also accepts responsibility for the study idea, experimental design, selection of tissues and regions of interest for generation of the tissue microarray, generation of figures, writing of the manuscript and performing some of the data analyses. All authors reviewed and approved the manuscript version to be published.

References

1. ElSayed NA, Aleppo G, Aroda VR et al (2023) 11. Chronic kidney disease and risk management: standards of care in diabetes – 2023. Diabetes Care 46(Suppl 1):S191–S202. https://doi.org/10.2337/dc23-S011
2. Lewis SM, Asselin-Labat ML, Nguyen Q et al (2021) Spatial omics and multiplexed imaging to explore cancer biology. Nat Methods 18(9):997–1012. https://doi.org/10.1038/s41592-021-01203-6
3. Hansen J, Sealfon R, Menon R et al (2022) A reference tissue atlas for the human kidney. Sci Adv 8(23):eabn4965. https://doi.org/10.1126/sciadv.abn4965
4. Neumann EK, Patterson NH, Rivera ES et al (2022) Highly multiplexed immunofluorescence of the human kidney using co-detection by indexing. Kidney Int 101(1):137–143. https://doi.org/10.1016/j.kint.2021.08.033
5. Hossain MS, Shahriar GM, Syeed MMM et al (2023) Region of interest (ROI) selection using vision transformer for automatic analysis using whole slide images. Sci Rep 13(1):11314. https://doi.org/10.1038/s41598-023-38109-6
6. Tervaert TW, Mooyaart AL, Amann K et al (2010) Pathologic classification of diabetic nephropathy. J Am Soc Nephrol 21(4):556–563. https://doi.org/10.1681/ASN.2010010010
7. Levey AS, Stevens LA, Schmid CH et al (2009) A new equation to estimate glomerular filtration rate. Ann Intern Med 150(9):604–612. https://doi.org/10.7326/0003-4819-150-9-200905050-00006
8. Goltsev Y, Samusik N, Kennedy-Darling J et al (2018) Deep profiling of mouse splenic architecture with CODEX multiplexed imaging. Cell 174(4):968-981.e915. https://doi.org/10.1016/j.cell.2018.07.010
9. Kretschmar C, Oyarzun C, Villablanca C et al (2016) Reduced adenosine uptake and its contribution to signaling that mediates profibrotic activation in renal tubular epithelial cells: implication in diabetic nephropathy. PLoS One 11(1):e0147430. https://doi.org/10.1371/journal.pone.0147430
10. SaratlijaNovakovic Z, GlavinaDurdov M, Puljak L et al (2012) The interstitial expression of alpha-smooth muscle actin in glomerulonephritis is associated with renal function. Med Sci Monit 18(4):CR235-240. https://doi.org/10.12659/msm.882623
11. Bobka S, Ebert N, Koertvely E et al (2018) Is early complement activation in renal transplantation associated with later graft outcome? Kidney Blood Press Res 43(5):1488–1504. https://doi.org/10.1159/000494014
12. Ma R, Cui Z, Hu SY et al (2014) The alternative pathway of complement activation may be involved in the renal damage of human anti-glomerular basement membrane disease. PLoS One 9(3):e91250. https://doi.org/10.1371/journal.pone.0091250
13. Pfister F, Vonbrunn E, Ries T et al (2020) Complement activation in kidneys of patients with COVID-19. Front Immunol 11:594849. https://doi.org/10.3389/fimmu.2020.594849
14. Liu T, Yang M, Xia Y et al (2021) Microarray-based analysis of renal complement components reveals a therapeutic target for lupus nephritis. Arthritis Res Ther 23(1):223. https://doi.org/10.1186/s13075-021-02605-9
15. Bus P, Chua JS, Klessens CQF et al (2018) Complement activation in patients with diabetic nephropathy. Kidney Int Rep 3(2):302–313. https://doi.org/10.1016/j.ekir.2017.10.005
16. Welsh-Bacic D, Lindenmeyer M, Cohen CD et al (2011) Expression of the chemokine receptor CCR6 in human renal inflammation. Nephrol Dial Transplant 26(4):1211–1220. https://doi.org/10.1093/ndt/gfq560
17. Pahl HL, Rosmarin AG, Tenen DG (1992) Characterization of the myeloid-specific CD11b promoter. Blood 79(4):865–870. https://doi.org/10.1182/blood.V79.4.865.bloodjournal794865
18. Jerke U, Rolle S, Dittmar G et al (2011) Complement receptor Mac-1 is an adaptor for NB1 (CD177)-mediated PR3-ANCA neutrophil activation. J Biol Chem 286(9):7070–7081. https://doi.org/10.1074/jbc.M110.171256
19. Pusztaszeri MP, Seelentag W, Bosman FT (2006) Immunohistochemical expression of endothelial markers CD31, CD34, von Willebrand factor, and Fli-1 in normal human tissues. J Histochem Cytochem 54(4):385–395. https://doi.org/10.1369/jhc.4A6514.2005
20. Al Barashdi MA, Ali A, McMullin MF, Mills K (2021) Protein tyrosine phosphatase receptor type C (PTPRC or CD45). J Clin Pathol 74(9):548–552. https://doi.org/10.1136/jclinpath-2020-206927
21. Gottfried E, Kunz-Schughart LA, Weber A et al (2008) Expression of CD68 in non-myeloid cell types. Scand J Immunol 67(5):453–463. https://doi.org/10.1111/j.1365-3083.2008.02091.x
22. Heidet L, Cai Y, Guicharnaud L, Antignac C, Gubler MC (2000) Glomerular expression of type IV collagen chains in normal and X-linked Alport syndrome kidneys. Am J Pathol 156(6):1901–1910. https://doi.org/10.1016/S0002-9440(10)65063-8
23. Singh N, Avigan ZM, Kliegel JA et al (2019) Development of a 2-dimensional atlas of the human kidney with imaging mass cytometry. JCI Insight 4(12):e129477. https://doi.org/10.1172/jci.insight.129477
24. Bek MJ, Reinhardt HC, Fischer KG et al (2003) Up-regulation of early growth response gene-1 via the CXCR3 receptor induces reactive oxygen species and inhibits Na^+/K^+-ATPase activity in an immortalized human proximal tubule cell line. J Immunol 170(2):931–940. https://doi.org/10.4049/jimmunol.170.2.931
25. Hoffmann U, Segerer S, Rummele P et al (2006) Expression of the chemokine receptor CXCR3 in human renal allografts – a prospective study. Nephrol Dial Transplant 21(5):1373–1381. https://doi.org/10.1093/ndt/gfk075
26. Hauser IA, Spiegler S, Kiss E et al (2005) Prediction of acute renal allograft rejection by urinary monokine induced by IFN-γ (MIG). J Am Soc Nephrol 16(6):1849–1858. https://doi.org/10.1681/ASN.2004100836

27. Lasagni L, Francalanci M, Annunziato F et al (2003) An alternatively spliced variant of CXCR3 mediates the inhibition of endothelial cell growth induced by IP-10, Mig, and I-TAC, and acts as functional receptor for platelet factor 4. J Exp Med 197(11):1537–1549. https://doi.org/10.1084/jem.20021897
28. Romagnani P, Beltrame C, Annunziato F et al (1999) Role for interactions between IP-10/Mig and CXCR3 in proliferative glomerulonephritis. J Am Soc Nephrol 10(12):2518–2526. https://doi.org/10.1681/ASN.V10122518
29. Romagnani P, Annunziato F, Lasagni L et al (2001) Cell cycle-dependent expression of CXC chemokine receptor 3 by endothelial cells mediates angiostatic activity. J Clin Invest 107(1):53–63. https://doi.org/10.1172/JCI9775
30. Trzpis M, Popa ER, McLaughlin PM et al (2007) Spatial and temporal expression patterns of the epithelial cell adhesion molecule (EpCAM/EGP-2) in developing and adult kidneys. Nephron Exp Nephrol 107(4):e119–e131. https://doi.org/10.1159/000111039
31. Seligson DB, Pantuck AJ, Liu X et al (2004) Epithelial cell adhesion molecule (KSA) expression: pathobiology and its role as an independent predictor of survival in renal cell carcinoma. Clin Cancer Res 10(8):2659–2669. https://doi.org/10.1158/1078-0432.ccr-1132-03
32. Zimpfer A, Maruschke M, Rehn S et al (2014) Prognostic and diagnostic implications of epithelial cell adhesion/activating molecule (EpCAM) expression in renal tumours: a retrospective clinicopathological study of 948 cases using tissue microarrays. BJU Int 114(2):296–302. https://doi.org/10.1111/bju.12487
33. Went PT, Lugli A, Meier S et al (2004) Frequent EpCam protein expression in human carcinomas. Hum Pathol 35(1):122–128. https://doi.org/10.1016/j.humpath.2003.08.026
34. Bix G, Iozzo RV (2008) Novel interactions of perlecan: unraveling perlecan's role in angiogenesis. Microsc Res Tech 71(5):339–348. https://doi.org/10.1002/jemt.20562
35. Bulow RD, Boor P (2019) Extracellular matrix in kidney fibrosis: more than just a scaffold. J Histochem Cytochem 67(9):643–661. https://doi.org/10.1369/0022155419849388
36. Gu X, Yang H, Sheng X et al (2021) Kidney disease genetic risk variants alter lysosomal beta-mannosidase (MANBA) expression and disease severity. Sci Transl Med 13(576):eaaz1458. https://doi.org/10.1126/scitranslmed.aaz1458
37. Ishii K, Kobayashi H, Taguchi K et al (2021) Kidney epithelial targeted mitochondrial transcription factor A deficiency results in progressive mitochondrial depletion associated with severe cystic disease. Kidney Int 99(3):657–670. https://doi.org/10.1016/j.kint.2020.10.013
38. Cao Y, Karsten U, Zerban H, Bannasch P (2000) Expression of MUC1, Thomsen-Friedenreich-related antigens, and cytokeratin 19 in human renal cell carcinomas and tubular clear cell lesions. Virchows Arch 436(2):119–126. https://doi.org/10.1007/pl00008210
39. Chalick M, Jacobi O, Pichinuk E et al (2016) MUC1-ARF – a novel muc1 protein that resides in the nucleus and is expressed by alternate reading frame translation of MUC1 mRNA. PLoS One 11(10):e0165031. https://doi.org/10.1371/journal.pone.0165031
40. Perry J, Ho M, Viero S, Zheng K, Jacobs R, Thorner PS (2007) The intermediate filament nestin is highly expressed in normal human podocytes and podocytes in glomerular disease. Pediatr Dev Pathol 10(5):369–382. https://doi.org/10.2350/06-11-0193.1
41. Bertelli E, Regoli M, Fonzi L et al (2007) Nestin expression in adult and developing human kidney. J Histochem Cytochem 55(4):411–421. https://doi.org/10.1369/jhc.6A7058.2007
42. Rutz S, Eidenschenk C, Kiefer JR, Ouyang W (2016) Post-translational regulation of RORγt – a therapeutic target for the modulation of interleukin-17-mediated responses in autoimmune diseases. Cytokine Growth Factor Rev 30:1–17. https://doi.org/10.1016/j.cytogfr.2016.07.004
43. Medvedev A, Yan ZH, Hirose T, Giguere V, Jetten AM (1996) Cloning of a cDNA encoding the murine orphan receptor RZR/RORγ and characterization of its response element. Gene 181(1–2):199–206. https://doi.org/10.1016/s0378-1119(96)00504-5
44. He YW, Deftos ML, Ojala EW, Bevan MJ (1998) RORγt, a novel isoform of an orphan receptor, negatively regulates Fas ligand expression and IL-2 production in T cells. Immunity 9(6):797–806. https://doi.org/10.1016/s1074-7613(00)80645-7
45. Xie Y, Sakatsume M, Nishi S, Narita I, Arakawa M, Gejyo F (2001) Expression, roles, receptors, and regulation of osteopontin in the kidney. Kidney Int 60(5):1645–1657. https://doi.org/10.1046/j.1523-1755.2001.00032.x
46. Hudkins KL, Giachelli CM, Cui Y, Couser WG, Johnson RJ, Alpers CE (1999) Osteopontin expression in fetal and mature human kidney. J Am Soc Nephrol 10(3):444–457. https://doi.org/10.1681/ASN.V103444
47. Brown LF, Berse B, Van de Water L et al (1992) Expression and distribution of osteopontin in human tissues: widespread association with luminal epithelial surfaces. Mol Biol Cell 3(10):1169–1180. https://doi.org/10.1091/mbc.3.10.1169
48. Shiiki H, Enomoto Y, Uyama H et al (1994) Distribution of thrombomodulin in patients with focal and segmental glomerulosclerosis (FSGS). Nihon Jinzo Gakkai Shi 36(8):890–895
49. van Aanhold CCL, Dijkstra KL, Bos M et al (2021) Reduced glomerular endothelial thrombomodulin is associated with glomerular macrophage infiltration in diabetic nephropathy. Am J Pathol 191(5):829–837. https://doi.org/10.1016/j.ajpath.2021.02.002
50. van Aanhold CCL, Bos M, MirabitoColafella KM et al (2021) Thrombomodulin is upregulated in the kidneys of women with pre-eclampsia. Sci Rep 11(1):5692. https://doi.org/10.1038/s41598-021-85040-9
51. Sengoelge G, Winnicki W, Kupczok A et al (2014) A SAGE based approach to human glomerular endothelium: defining the transcriptome, finding a novel molecule and highlighting endothelial diversity. BMC Genomics 15(1):725. https://doi.org/10.1186/1471-2164-15-725